Mechanisms of molecular doping of graphene: A first-principles study

Srijan Kumar Saha,[1,2] Reddy Ch. Chandrakanth,[3] H. R. Krishnamurthy,[1,2] and U. V. Waghmare[3]
[1]*Center for Condensed Matter Theory, Department of Physics, Indian Institute of Science, Bangalore 560012, India*
[2]*Condensed Matter Theory Unit, Jawaharlal Nehru Centre for Advanced Scientific Research, Bangalore 560064, India*
[3]*Theoretical Sciences Unit, Jawaharlal Nehru Centre for Advanced Scientific Research, Bangalore 560064, India*
(Received 20 March 2009; revised manuscript received 28 August 2009; published 5 October 2009)

Doping graphene with electron donating or accepting molecules is an interesting approach to introduce carriers into it, analogous to electrochemical doping accomplished in graphene when used in a field-effect transistor. Here, we use first-principles density-functional theory to determine changes in the electronic-structure and vibrational properties of graphene that arise from the adsorption of aromatic molecules such as aniline and nitrobenzene. Identifying the roles of various mechanisms of chemical interaction between graphene and a molecule, we bring out the contrast between electrochemical and molecular doping of graphene. Our estimates of various contributions to shifts in the Raman-active modes of graphene with molecular doping are fundamental to the possible use of Raman spectroscopy in (a) characterization of the nature and concentration of carriers in graphene with molecular doping, and (b) graphene-based chemical sensors.

DOI: 10.1103/PhysRevB.80.155414 PACS number(s): 81.05.Uw, 71.15.Mb, 63.20.−e, 78.30.−j

I. INTRODUCTION

A variety of exotic properties and potential applications of graphene, a two-dimensional honeycomb lattice of carbon, have triggered an intense research activity since its experimental realization.[1] Analogous to semiconductors, the possibility to dope graphene heavily either by gate voltage or molecular adsorption is of particular interest to applications in electronics and chemical sensors based on graphene. It has been shown recently that the phonons of graphene are altered interestingly by tuning the applied gate voltage[2,3] and that Raman spectroscopy can be used to measure the nature and level of doping-induced carriers. Molecular doping and the related chemical sensor properties of graphene have also been studied both experimentally and theoretically.[4,5] A recent experiment[4] has demonstrated graphene's potential for solid-state gas sensors with an ultimate sensitivity that permits detection of even an individual molecule.

The interaction of a single-wall carbon nanotube (SWCNT) with molecules[6] and metal nanoparticles[7] is known to result in significant changes in the electronic properties of the SWCNT. It is of fundamental interest to ask whether interactions with adsorbed molecules would similarly affect the electronic properties of graphene, in particular, its linear electronic dispersion at the Fermi energy, known as the Dirac cone and responsible for its exotic properties. The Dirac cone in graphene is also responsible for the strong sensitivity of its vibrations to small changes in its electronic structure. Hence, Raman spectra of molecular-doped graphene could show characteristic features corresponding to various aspects of the interaction of the adsorbed molecules with graphene and is expected to be a valuable tool in its investigation.

As mentioned above, molecular doping of graphene is usually achieved by adsorbing molecules onto the host graphene lattice. The adsorbate molecules either release electrons to the graphene (*n*-type doping) or remove them from the graphene (*p*-type doping), depending on their electron donating or accepting ability. This charge transfer and associated shift in the Fermi level influence the transport properties of graphene. While the gate voltage controls the level of electrochemical doping in graphene, the concentration of carriers introduced in molecular doping is controlled by changing the coverage of adsorbate molecules. If charge transfer is the only dominant feature resulting from adsorption, then the dependence of the Fermi energy ϵ_F on the adsorbate coverage can be determined, assuming the linear dispersion near Dirac point, via[8,9]

$$\epsilon_F = \mathrm{sgn}(\sigma)\hbar v_F\sqrt{\pi|\sigma|} = \mathrm{sgn}(f)\hbar v_F\sqrt{\pi n_s|f|}, \qquad (1)$$

where σ is the layer charge concentration, f is the amount of charge transferred per molecule, and n_s is the coverage—the number of molecules adsrobed per unit area and $\hbar v_F = 5.53$ eV Å [from density-functional theory (DFT) calculation[10]]. However, many other effects such as adsorbate-adsorbate interaction, adsorbate-graphene interaction, thermally excited (even at room temperature) site promotion (surface diffusion), unintentional doping, etc., can influence the vibrational and transport properties of graphene as well. Vibrational properties as measured with Raman or other spectroscopies can be used to characterize these mechanisms.

Motivated by these considerations, we study here the interplay between electronic-structure and vibrational properties of molecular-doped graphene, particularly by aromatic organic molecules such as aniline ($C_6H_5NH_2$) and nitrobenzene ($C_6H_5NO_2$), using first-principles calculations based on DFT.

The paper is organized as follows. In Sec. II, we briefly describe the technical aspects of our first-principles calculations. Section III presents our results together with the discussion of the underlying physics. Finally, Sec. IV contains some concluding remarks.

II. METHODOLOGY

We use the PWSCF (Ref. 11) implementation of DFT, with a plane-wave basis set and ultrasoft pseudopotentials.[12] We

adopt the exchange-correlation functional of Perdew-Zunger[13] for the local-density approximation (LDA) and that of Perdew-Burke-Ernzerhof[14] for the generalized gradient approximation (GGA). A supercell geometry with a vacuum larger than 16 Å in the z direction is used to ensure negligible interaction between one graphene layer and its periodic images. Molecules are placed on one side of the graphene surface. Kohn-Sham wave functions are represented using a plane-wave basis truncated at an energy cutoff of 40 Ry. Such a high cutoff[15] is used to include a large number of plane waves in the calculation as some of our results are quite sensitive to the energy cutoff, generally expected when relatively long-ranged forces play a significant role in the adsorption. The Brillouin-zone integration is sampled on uniform Monkhorst-Pack[16] grids, of sizes $12\times12\times1$ and $6\times6\times1$ k points, respectively, for 3×3 and 5×5 supercells of graphene. Such dense grids are essential to produce accurate descriptions of phonons exhibiting a large Kohn anomaly as in graphene. For occupation of states, we use the Fermi-Dirac distribution with a smearing of 0.01 Ry.[17] Structural relaxation is carried out in each case to minimize energy using the Broyden-Flecher-Goldfarb-Shanno-based method.[18] Phonon frequencies are calculated using the density-functional perturbation theory[19] within the standard Born-Oppenheimer (BO) approximation, and then time-dependent perturbation theory is used to estimate the effect of dynamic corrections beyond the BO approximation.

III. RESULTS AND DISCUSSION

For sparsely layered systems such as graphite, with predominantly van-der-Waals interlayer interactions, standard DFT-based approaches such as LDA and GGA are known to yield poor predictions for interlayer spacings.[20,21] However, in case of graphite, LDA fortuitously gives reasonable interlayer spacing while GGA shows negligible binding at the measured spacing.[22–24] Our LDA estimates of the equilibrium in-plane lattice spacing ($a_0^{\mathrm{LDA}}=2.4394$ Å) and interlayer distance ($d_0^{\mathrm{LDA}}=3.2932$ Å) of AB-stacked graphite are close to the respective experimental[25] values $a_0^{\mathrm{expt}}=2.46$ Å and $d_0^{\mathrm{expt}}=3.35$ Å. While the GGA can reproduce the experimental a_0, it gives a too large d_0 (4.2415 Å). In this work, we use both LDA and GGA to obtain upper and lower bounds for adsorption energies and related properties.

We investigate the interaction of aniline (electron donor) and nitrobenzene (electron acceptor) with graphene for two different coverages—a high-density phase (3×3 supercell) with one molecule per 18 carbon atoms and a low-density phase (5×5 supercell) with one molecule per 50 carbon atoms. Since both adsorbates have closed valence shells, we perform nonspin-polarized calculations. The adsorption energy E_{ads} is obtained (by definition) as

$$E_{\mathrm{ads}} = E_{\mathrm{gra}} + E_{\mathrm{mol}} - E_{\mathrm{gra+mol}}, \tag{2}$$

where E_{gra}, E_{mol}, and $E_{\mathrm{gra+mol}}$ are the relaxed energy, respectively, for graphene, the molecule, and the combined system. We consider various possible sites of adsorption and orientations of the phenyl ring with respect to the hexagonal rings of graphene; configurations with their molecular planes parallel and perpendicular to the graphene surface are also considered. We find (see Fig. 1) that the lowest-energy configurations in case of aniline correspond to "atop site" adsorption at high coverage and "bridge site" adsorption at low coverage whereas in case of nitrobenzene they correspond to "hollow site" adsorption for both high and low coverage. Interestingly, in all these lowest-energy configurations, the plane of aniline or nitrobenzene is not exactly parallel to graphene layer but is tilted slightly. The adsorption energies, adsorbate-graphene distances, and angles of tilting are listed in Table I. The distance (tilt angle) between the planes of graphene and a molecule depends on the chemistry as well as the coverage, and is somewhat overestimated (underestimated) in GGA relative to LDA.

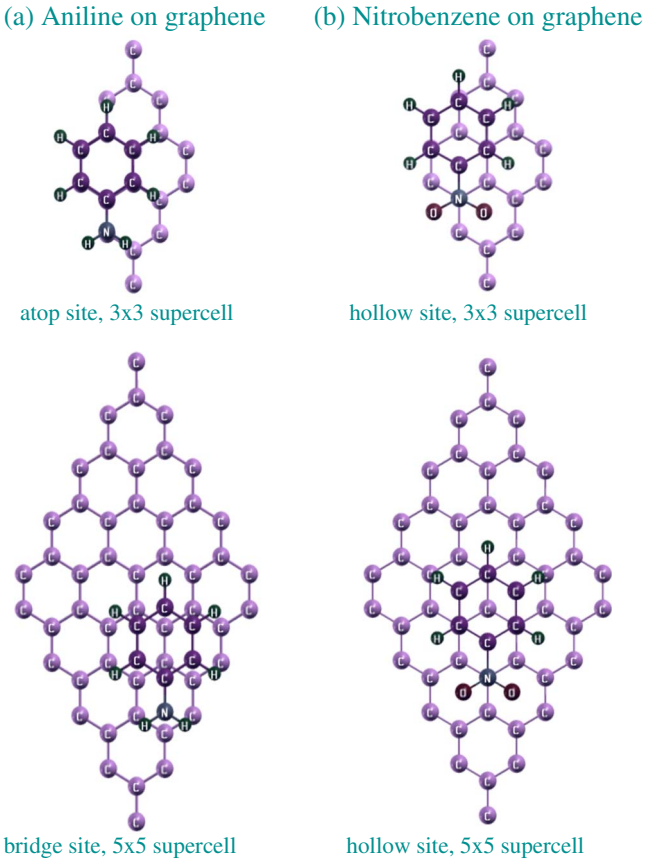

FIG. 1. (Color online) Top view of the lowest-energy configurations of the molecules adsorbed on graphene.

For all of the perpendicular configurations considered, we find that the adsorption energies are much smaller [by atleast 0.1 eV/molecule (in LDA)] than for any configuration where the phenyl ring is almost parallel to the graphene plane (i.e., parallel configuration is energetically more favorable). This suggests that the π-π stacking is an important ingredient in the stability and adsorption of these aromatic molecules. It is also found that the adsorption energies of each molecule in the atop-, hollow-, and bridge-site configurations, with orientation parallel to graphene, are quite close to each other (in some cases the difference is less than 0.04 eV/molecule). Such small differences in energy may lead to site migration even at room temperature. In each of the above cases, the molecule was initially placed about 2.5 Å away from the

TABLE I. Distance and angle of tilting between the planes of molecule and graphene, and associated adsorption energies for the coverages of one molecule per 3×3 and 5×5 supercell of graphene.

	Aniline				Nitrobenzene			
	LDA (3×3)	GGA (3×3)	LDA (5×5)	GGA (5×5)	LDA (3×3)	GGA (3×3)	LDA (5×5)	GGA (5×5)
Adsorption energy (eV/molecule)	0.413	0.052	0.341	0.041	0.516	0.072	0.412	0.051
Adsorbate-sheet distance (Å)	3.3–4.7	4.1–5.8	3.5–4.9	4.3–6.0	3.0–4.1	3.9–5.3	3.2–4.3	4.1–5.5
Angle of tilting (deg)	5.3	2.3	3.0	1.4	10.0	4.5	5.8	2.7

graphene surface and the whole system was then allowed to relax. During relaxation the molecules moved away from the surface, which clearly shows that only weak bonds are formed between graphene and molecules (i.e., both molecules physisorb on graphene). At both coverages, the amino group of aniline moves further away from the graphene surface than its phenyl ring, indicating a weaker interaction of the surface with the amino group than with the phenyl ring. In contrast, in case of nitrobenzene, the tilting of its nitro group toward the graphene surface indicates that the nitro group-surface interaction is relatively stronger. Accordingly, the adsorption energy for nitrobenzene is larger than that for aniline. It is thus evident that the type of functional group crucially affects the adsorption process. Since the tilting of the molecules occurs at both high and low coverages, we conclude that it results primarily from the adsorbate-surface interaction rather than the coverage-dependent interadsorbate interaction or steric hindrance.

For both choices of DFT functionals (LDA and GGA), we find that the overall physical pictures are similar but the effects in GGA are weaker than LDA. When compared with LDA, GGA yields much lower adsorption energies ($\frac{1}{6}-\frac{1}{9}$th of the LDA values) as the adsorbate molecules get placed 0.8–1.7 Å further away from the graphene sheet, quite expected as GGA is known[22–24] to give embarassingly small off-plane binding in graphetic materials. As GGA leads to much weaker interaction between molecules and graphene, we use LDA in our analysis of phonons.

NH_2 being an electropositive group, aniline is expected to be a charge donor. If charge donation is the only dominant process during adsorption, the graphene lattice should expand with the extra electrons. We find a small charge transfer toward graphene surface, but no discernible lattice expansion, because the charge-transfer-induced stress gets largely compensated by the aniline-graphene interaction, with the NH_2 group moving away from the graphene surface. This cancellation is found at both the low and high coverages. The electronic density of states (see Fig. 3) shows that the highest-occupied molecular orbital (HOMO) of aniline is inside the graphene's valence band and completely filled while its lowest-unoccupied molecular orbital (LUMO) is high in the conduction band and completely empty, and no discernible upshift in the Fermi energy is found [see Figs. 3 and 4], in spite of a small charge transfer [Fig. 2(a)].

Similarly, nitrobenzene is expected to be a charge acceptor owing to its electronegative NO_2 group, causing the graphene lattice to shrink due to the resulting hole doping. However, we do not find any discernible charge transfer at either high or low coverages [Fig. 2(b)]. Furthermore, a significant lattice expansion is found at high coverage because of strong interadsorbate repulsion and this decreases with decreasing coverage. At the coverage corresponding to 3×3 supercell, we find a lattice expansion of 0.14% and a downshift of 0.25 eV in the Fermi energy. The HOMO of nitrobenzene is deep inside the graphene valence band while its LUMO in the conduction band is relatively closer to the Fermi level, resulting in a relatively larger hybridization and the Fermi energy shift of 0.25 eV into the valence band [see Figs. 3 and 4] However, this downshift does not arise from the charge-transfer-induced hole doping but mainly arises from the lattice expansion associated with adsorbate-adsorbate interaction and adsorbate-graphene (in particular, simple electrostatic) interaction.

Table II shows our estimates for the shifts in frequency of the Raman *G* band, calculated within the adiabatic BO (static) approximation. These do not agree with the experimental results[26] (also listed in Table II) even as regards the trends with increasing coverage (the values of the coverage in the experiments are not clearly known). However, due to the strong electron-phonon coupling in graphene, the adiabatic approximation has been demonstrated to be inadequate in describing the doping dependence of Raman *G* band in graphene, both theoretically and experimentally.[2,9] Physically, the electron dynamics and the vibrational motion of

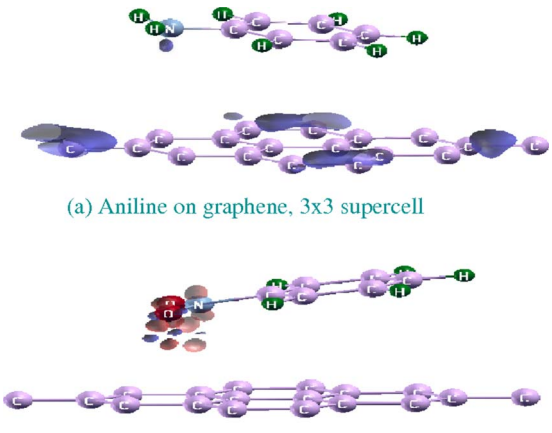

FIG. 2. (Color online) The transfer of charge (blue in color) between the molecule and graphene as evident in the difference in charge density between molecule-graphene complex and graphene and molecule: $\rho_{(\text{graphene+molecule})}-\rho_{\text{graphene}}-\rho_{\text{molecule}}$.

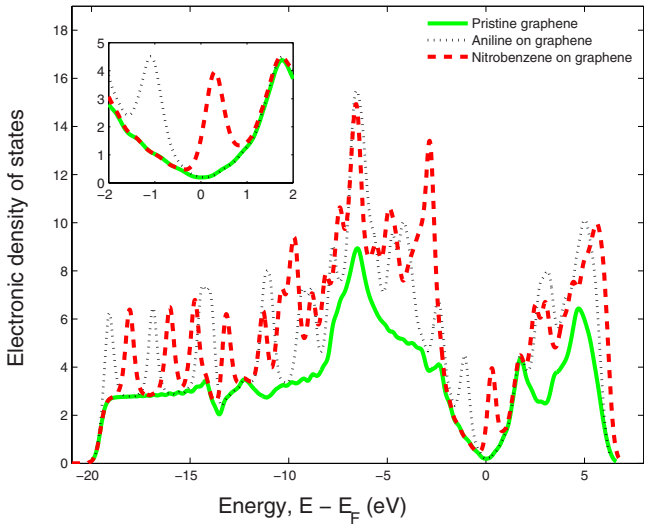

FIG. 3. (Color online) Electronic density of states of pristine graphene, aniline-adsorbed grapheme, and nitrobenzene-adsorbed graphene, for the high coverage of one molecule per 3×3 supercell.

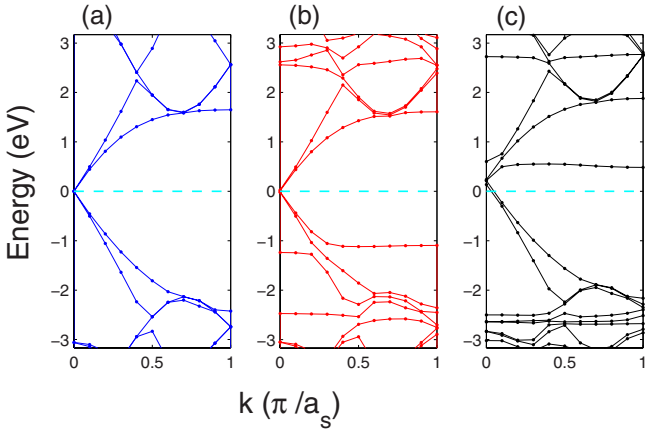

FIG. 4. (Color online) Electronic structure of the (a) pristine single-layer graphene, (b) aniline-adsorbed graphene, and (c) nitrobenzene-adsorbed graphene (for 3×3 supercell). The Dirac cone at the **K** point of one unit cell maps onto that at the Γ point of 3×3 supercell configuration. In both of these adsorption cases, the band structure is not much affected (i.e., the mixing between graphene band and molecular level is small) and hence the rigid-band theory is applicable, as has been discussed before in the context of graphite intercalation compounds (Ref. 27).

nuclei occur at comparable time scales and cannot be decoupled. We treat dynamical effects arising at small doping within the time-dependent perturbation theory.[9] We note that the electron dispersion around the Dirac point continues to be linear in molecularly doped graphene, up to half an eV of the Fermi energy (see Fig. 4). Hence, the change in the Raman *G*-band phonon energy at zero temperature is given by[8,9]

$$\hbar\Delta\omega_{\Gamma}^{\text{dynamic}} = \alpha_{\Gamma}|\epsilon_F| + \frac{\alpha_{\Gamma}\hbar\omega_{\Gamma}^{\text{static}}(0)}{4}\ln\left|\frac{2|\epsilon_F| - \hbar\omega_{\Gamma}^{\text{static}}(0)}{2|\epsilon_F| + \hbar\omega_{\Gamma}^{\text{static}}(0)}\right|, \tag{3}$$

where $\alpha_{\Gamma}=\frac{2A_0\langle g_{\Gamma}^2\rangle_F}{\pi\hbar^2 v_F^2}=36.0\ \text{cm}^{-1}/\text{eV}$ (our DFT value, in excellent agreement with Ref. 9) and A_0 is the equilibrium unit-cell area. In this case, the frequency shift diverges logarithmically in the limit when the magnitude of the shift in the Fermi energy is half of the phonon energy and increases in proportion to the shift in Fermi energy for $|\epsilon_F|>\hbar\omega_0^{\text{static}}/2$ as long as the effect of the charge doping can be considered as a perturbation. Consistent with the results shown in Fig. 4 and emphasized earlier, we take the Fermi velocity and the value of α_{Γ} to be the same as for pristine graphene. It is clear from Table II that with the inclusion of the dynamic corrections, the trends in our estimated phonon frequencies with coverage agrees dramatically better with experimental measurements.[26] We note that dynamic effects are stronger in

TABLE II. Phonon frequency of the Raman *G* band of graphene when aniline and nitrobenzene are adsorbed on it with coverages of 1 molecule per 3×3 (high coverage) and 5×5 (low coverage) supercells. Our LDA frequencies are slightly and systematically higher than the experimental values, consistent with the LDA's general tendency to overestimate the phonon frequencies owing to its well-known overbinding nature. Here we also attach the experimental results (Ref. 26) to show the qualitative trend. Note that a direct comparison is not possible as the estimates of the coverage corresponding to experimental results (Ref. 26) are not available.

	LDA Phonon frequency (cm^{-1})			Experimental results (from Ref. 26)	
System	Constant lattice	Optimized lattice	After adding dynamic effect	Hammet σ substituent constant	Frequency (cm^{-1})
Nitrobenzene on graphene					
High coverage	1603	1596	1605	0.80	1587
Low coverage	1602	1599	1603	0.30	1580
Pristine graphene					
	1602	1602	1602	0.00	1573
Aniline on graphene					
Low coverage	1602	1602	1601	−0.27	1569
High coverage	1602	1602	1600	−0.67	1566

TABLE III. Frequencies of molecular vibrations for aniline and nitrobenzene that change noticeably when adsorbed on graphene with coverages of one molecule per 3×3 and 5×5 supercells. Experimental data are taken from Ref. 28 (Aniline) and from Ref. 29 (Nitrobenzene). Considering the facts that the experimental values are not corrected for anharmonic effects, and that the LDA has a general tendency to overbind, our calculated static frequencies of both isolated molecules are in good agreement with experiments.

	Isolated molecule			5×5 supercell	3×3 supercell
	Assignment	Experimental frequency (cm^{-1})	Static LDA frequency (cm^{-1})	Static LDA frequency (cm^{-1})	Static LDA frequency (cm^{-1})
Aniline	NH_2 asymmetric stretching	3500	3666	3665	3621
	NH_2 symmetric stretching	3418	3543	3540	3499
	CH stretching	3089	3109	3099	3076
	CH stretching	3074	3093	3080	3065
	CH stretching	3053	3083	3075	3061
	CH stretching	3041	3061	3057	3050
	CH stretching	3025	3061	3057	3043
Nitrobenzene	NO_2 asymmetric stretching	1548	1598	1579	1553
	CH stretching	3050	3088	3078	3086
	CH stretching	3080	3100	3092	3104
	CH stretching	3080	3106	3097	3106
	CH stretching	3080	3119	3110	3115
	CH stretching	3080	3121	3111	3117

the case of nitrobenzene, owing to the greater shift in the Fermi energy with its adsorption.

Finally, we note that the changes due to molecular doping in the frequency of the Raman 2D band, determined by phonons at $\mathbf{K}+\Delta\mathbf{K}$, can be inferred from our results for the Γ-point phonons for the low-coverage 5×5 supercell (because of zone folding). We find that graphene's 2D band gets upshifted by 1.5 and 8.8 cm^{-1} upon adsorption of aniline and nitrobenzene, respectively. These trends are in agreement with the experimental observation.[26] Furthermore, the spectrum of Γ-point phonons of the 3×3 supercell gives us a direct access to the **K**-point phonon. At this coverage, graphene's **K**-point phonon (1336.6 cm^{-1}) shifts to 1338.3 and 1345.2 cm^{-1}, respectively, with the adsorption of aniline and nitrobenzene. Interestingly, frequencies of certain optically active molecular vibrations also change significantly upon adsorption on graphene (see Table III). While going from isolated molecule to 5×5 coverage to 3×3 coverage, most of the listed vibrational modes exhibit a noticeable downward trend in their frequency shifts both for aniline and nitrobenzene but only in the case of nitrobenezene, as we go from 5×5 to 3×3 coverage, CH stretch modes show upward frequency shifts. The obtained shifts in the vibrational frequencies can mainly be attributed to the way vibrational motion of a particular mode gets modified with coverage, depending on the interplay of different repulsive and attractive forces. More interestingly, for both molecules, an infrared-active vibrational mode which involves the asymmetric stretching of functional group exhibits large frequency shifts in common (see Table III and Fig. 5). This could also be exploited in applications of graphene in molecular sensors.

IV. CONCLUSIONS

In conclusion, we have uncovered various facets of the interaction of aniline and nitrobenzene with graphene, identifying their signatures in electronic-structure and vibrational spectra. We have shown that the linear dispersion in the Dirac-cone electronic structure of graphene is preserved upon molecular adsorption. At a fundamental level, we have shown that the resulting changes in the vibrational spectra of graphene arise from various competing mechanisms such as charge-transfer adsorption-induced expansion of the graphene lattice, intermolecular interactions, and

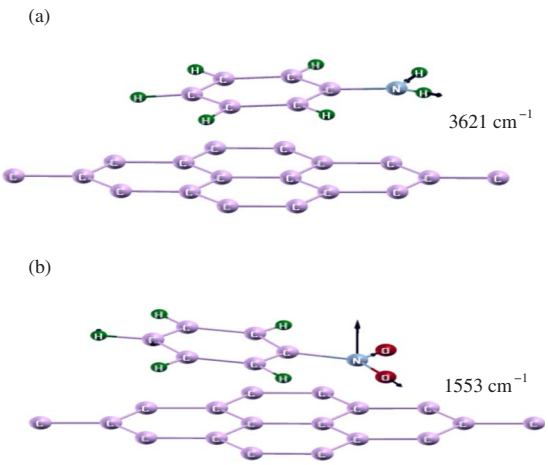

FIG. 5. (Color online) Atomic displacements in the normal modes of (a) aniline-adsorbed and (b) nitrobenzene-adsorbed graphene (for coverage of one molecule per 3×3 supercell).

dynamic response, and that dynamic corrections beyond Born-Oppenheimer approximation are essential to understand the observed[26] vibrational spectra of molecularly doped graphene. This work shows the importance of dynamic corrections to the phonon frequencies of molecular-doped graphene—which we have previously shown to be crucial for electrochemical doping[3] and substitutional doping[30] by boron or nitrogen as well; and brings out the underlying contrast between the electrochemical and the molecular doping of graphene. Our results will be useful in characterization of doping in graphene achieved with molecular adsorption.

ACKNOWLEDGMENTS

We thank C. N. R. Rao for suggesting this problem and encouragement. S.K.S. gratefully acknowledges financial support from the Condensed Matter Theory Unit at JNCASR. We would also like to acknowledge use of central computing facility from the Centre for Computational Materials Science at JNCASR.

[1] K. S. Novoselov, A. K. Geim, S. V. Morozov, D. Jiang, Y. Zhang, S. V. Dubonos, I. V. Grigorieva, and A. A. Firsov, Science **306**, 666 (2004).
[2] S. Pisana, M. Lazzeri, C. Casiraghi, K. S. Novoselov, A. K. Geim, A. C. Ferrari, and F. Mauri, Nature Mater. **6**, 198 (2007).
[3] A. Das, S. Pisana, B. Chakraborty, S. Piscanec, S. K. Saha, U. V. Waghmare, K. S. Novoselov, H. R. Krishnamurthy, A. K. Geim, A. C. Ferrari, and A. K. Sood, Nat. Nanotechnol. **3**, 210 (2008).
[4] F. Schedin, A. K. Geim, S. V. Morozov, E. W. Hill, P. Blake, M. I. Katsnelson, and K. S. Novoselov, Nature Mater. **6**, 652 (2007).
[5] T. O. Wehling, K. S. Novoselov, S. V. Morozov, E. E. Vdovin, M. I. Katsnelson, A. K. Geim, and A. I. Lichtenstien, Nano Lett. **8**, 173 (2008).
[6] H. Shin, S. M. Kim, S. Yoon, A. Benayad, K. K. Kim, S. J. Kim, H. K. Park, J. Choi, and Y. H. Lee, J. Am. Chem. Soc. **130**, 2062 (2008).
[7] R. Voggu, S. Pal, S. K. Pati, and C. N. R. Rao, J. Phys.: Condens. Matter **20**, 215211 (2008).
[8] T. Ando, J. Phys. Soc. Jpn. **75**, 124701 (2006).
[9] M. Lazzeri and F. Mauri, Phys. Rev. Lett. **97**, 266407 (2006).
[10] S. K. Saha, U. V. Waghmare, H. R. Krishnamurthy, and A. K. Sood, Phys. Rev. B **76**, 201404(R) (2007).
[11] S. Baroni, S. de Gironcoli, A. Dal Corso, and P. Giannozzi, http://www.pwscf.org
[12] D. Vanderbilt, Phys. Rev. B **41**, 7892 (1990).
[13] J. P. Perdew and A. Zunger, Phys. Rev. B **23**, 5048 (1981).
[14] J. P. Perdew, K. Burke, and M. Ernzerhof, Phys. Rev. Lett. **77**, 3865 (1996).
[15] S. K. Saha, U. V. Waghmare, H. R. Krishnamurthy, and A. K. Sood, Phys. Rev. B **78**, 165421 (2008).
[16] H. J. Monkhorst and J. D. Pack, Phys. Rev. B **13**, 5188 (1976).
[17] S. de Gironcoli, Phys. Rev. B **51**, 6773 (1995).
[18] http://www.library.cornell.edu/nr/bookcpdf/c10-7.pdf
[19] S. Baroni, S. de Gironcoli, A. Dal Corso, and P. Giannozzi, Rev. Mod. Phys. **73**, 515 (2001).
[20] D. P. DiVincenzo, E. J. Mele, and N. A. W. Holzwarth, Phys. Rev. B **27**, 2458 (1983).
[21] L. A. Girifalco and M. Hodak, Phys. Rev. B **65**, 125404 (2002).
[22] J. C. Charlier, X. Gonze, and J. P. Michenaud, Phys. Rev. B **43**, 4579 (1991); Carbon **32**, 289 (1994).
[23] N. Ooi, A. Rairkar, and J. B. Adams, Carbon **44**, 231 (2006).
[24] N. Mounet and N. Marzari, Phys. Rev. B **71**, 205214 (2005).
[25] F. Tuinstra and J. L. Koenig, J. Chem. Phys. **53**, 1126 (1970).
[26] B. Das, R. Voggu, C. S. Rout, and C. N. R. Rao, Chem. Commun. (Cambridge) **2008**, 5155.
[27] G. Sun, M. Kertesz, J. Kürti, and R. H. Baughman, Phys. Rev. B **68**, 125411 (2003).
[28] E. Akalin and S. Akyüz, J. Mol. Struct. **482-483**, 175 (1999), and references therein.
[29] A. Dal Corso, Phys. Rev. B **64**, 235118 (2001), and references therein.
[30] L. S. Panchakarla, K. S. Subrahmanyam, S. K. Saha, A. Govindaraj, H. R. Krishnamurthy, U. V. Waghmare, and C. N. R. Rao, Adv. Mater. (to be published 2009).